Using Quasi-Elastic Events to Estimate the Neutrino Flux of the MINOS Experiment

Mark Dorman

First Year Report, Summer 2005

Abstract

A review of the MINOS experiment and it's physics goals is given. The need for an accurate measurement of the neutrino flux is justified and a method for this measurement involving quasi-elastic neutrino-nucleon interactions is presented. A quasi-elastic event sample selection based upon a number of discriminating variables and a maximum likelihood analysis is developed and results are shown for a large Monte Carlo event set. The sample selection is applied to real data from the MINOS near detector as well as a corresponding Monte Carlo data set and some comparisons of physics quantities are presented.

1 Introduction

The phenomenology of weak interactions has come a long way since Pauli's 'Dear Radioactive Ladies and Gentlemen' letter of 1930 and Fermi's pointlike four fermion interaction model of nuclear β-decay but there are still experimental results that cannot be explained within the standard model of particle physics. One such set of observations became known as the *atmospheric neutrino anomaly* and showed a discrepancy in the numbers of electron and muon neutrinos arriving at the Earth's surface. Cosmic rays incident on the upper atmosphere interact with molecular nucleons and produce a cascade of secondary particles including large numbers of pions which subsequently decay as follows (predominantly):

$$\pi^{\pm} \rightarrow \mu^{\pm} + \nu_{\mu}(\overline{\nu}_{\mu}) \tag{1}$$

$$\mu^{\pm} \rightarrow e^{\pm} + \nu_{e}(\overline{\nu}_{e}) + \overline{\nu}_{\mu}(\nu_{\mu}) \tag{2}$$

To first order the ratio of $\nu_{\mu}(\overline{\nu}_{\mu})$:$\nu_{e}(\overline{\nu}_{e})$ arriving should be 2:1, however, both water Cerenkov experiments such as Super-Kamiokande [1] and iron sampling calorimeter experiments such as Soudan-2 [2] measured a deficit in the numbers of ν_{μ}. The solution, suggested by Pontecorvo in 1967 [3], was that the mass eigenstates of neutrinos are not the same as the weak eigenstates that participate in the weak interaction and correspondingly that neutrinos have mass. As such, leptonic flavour mixing can occur in charged current processes via interactions of the form:

$$\bar{\nu}_{L\alpha}V^{(l)}_{\alpha\beta}\gamma^{\mu}\hat{e}_{L\beta}\hat{W}_{\mu} + h.c. \tag{3}$$

where $\alpha, \beta \in (e, \mu, \tau)$, the subscript L denotes left handed chiral fields and $V^{(l)}_{\alpha\beta}$ is the Maki-Nakagawa-Sakata (MNS) unitary lepton mixing matrix (in analogy with the CKM matrix in the quark sector) and a neutrino produced in a weak interaction will consist of a linear superposition of the mass eigenstates ν_i where $i \in (1, 2, 3, \ldots)$[1]:

$$|\nu_\alpha\rangle = \sum_i V^*_{\alpha i}|\nu_i\rangle \tag{4}$$

It is the phenomena of neutrino flavour change (or *oscillation*) that can explain the missing atmospheric ν_μ and it is the parameters that govern neutrino oscillations that are being investigated by the MINOS (Main Injector Neutrino Oscillation Search) experiment.

2 Neutrino Oscillations

To understand the origin of neutrino oscillations in vacuum consider a neutrino that is initially in the state ν_α as defined in (4) and apply the Schrödinger equation to the i^{th} component in its rest frame to see that the time evolution of this initial state component is:

$$|\nu_i(\tau_i)\rangle = e^{-im_i\tau_i}|\nu_i(0)\rangle \tag{5}$$

where m_i is the mass of ν_i and τ_i the time in the frame of that component. This Lorentz invariant phase factor may be re-written in terms of the time t and position L in the laboratory frame and the energy E_i and momentum p_i of the ν_i component in this frame:

$$\exp(-im_i\tau_i) = \exp(-i(E_it - p_iL)) = \exp(-i(E_i - p_i)L) \tag{6}$$

where (6) follows as the neutrino is, in practice, highly relativistic with $t \approx L$. Then assuming a definite common momentum p for all the components of ν_α and $m_i \ll p$:

$$E_i^2 = p^2 + m_i^2 \Rightarrow E_i \approx p + m_i^2/2p \tag{7}$$

So putting this into (4) and using $E \approx p$ as the average energy of the components of ν_α gives:

$$|\nu_\alpha(L)\rangle \approx \sum_i V^*_{\alpha i}e^{-i(m_i^2/2E)L}|\nu_i\rangle \tag{8}$$

[1] There is evidence to suggest that there may be more than 3 neutrino mass eigenstates. Any further mass eigenstates would not have a charged lepton partner and have no couplings to standard model $W^{\pm}$ or Z^0 bosons earning them the title *sterile* neutrinos.

Then using the unitarity of the MNS matrix to invert (4) and inserting the result into the above equation yields:

$$|\nu_\alpha(L)\rangle \approx \sum_\beta \left[\sum_i V^*_{\alpha i} e^{-i(m_i^2/2E)L} V_{\beta i} \right] |\nu_\beta\rangle \tag{9}$$

It can be seen from (9) that a neutrino born of flavour α and travelling a distance L will become a superposition of all the flavours. The probability, $P(\nu_\alpha \to \nu_\beta)$, of this ν_α being of flavour β after travelling a distance L is given by $|\langle \nu_\beta | \nu_\alpha(L) \rangle|^2$. Using the unitarity of the MNS matrix and (9) this may be written:

$$\begin{aligned} P(\nu_\alpha \to \nu_\beta) = \delta_{\alpha\beta} \quad & - \quad 4 \sum_{i>j} \mathcal{R}\,(V^*_{\alpha i} V_{\beta i} V_{\alpha j} V^*_{\beta j}) sin^2[1.27 \Delta m^2_{ij}(L/E)] \\ & + \quad 2 \sum_{i>j} \mathcal{I}\,(V^*_{\alpha i} V_{\beta i} V_{\alpha j} V^*_{\beta j}) sin[2.54 \Delta m^2_{ij}(L/E)] \end{aligned} \tag{10}$$

where $\Delta m^2_{ij} \equiv m_i^2 - m_j^2$ and the sine terms come from the relation:

$$\Delta m^2_{ij}(L/4E) \simeq 1.27 \Delta m^2_{ij}(\mathrm{eV}^2) \frac{L(\mathrm{km})}{E(\mathrm{GeV})} \tag{11}$$

It is not known at present the hierarchical structure (in mass) of the various neutrino mass eigenstates relative to each other but it is thought that one of the mass splittings, denoted here by ΔM^2, is much larger than the other(s). In the case of an oscillation experiment that has $\Delta M^2 L/E = \mathcal{O}(1)$ equation (11) can be simplified to:

$$P(\nu_\alpha \to \nu_\beta) \simeq 4 \left| \sum_{i\pm} V^*_{\alpha i} V_{\beta i} \right|^2 sin^2[1.27 \Delta M^2 (L/E)] \qquad (\alpha \neq \beta) \tag{12}$$

where the notation $i\pm$ means a sum over those mass eigenstates that lie above or below ΔM^2. The situation described above is known as *one mass scale dominance* [4] and implies that an experiment with such an L/E can only resolve the large ΔM^2 with any other neutrinos above it appearing as a single neutrino and any below it as a single neutrino.

The above forms can also be applied to situations in which only two mass eigenstates (and hence two linear combinations of flavour eigenstates) and a single mass splitting, Δm^2, are important. Such situations can arise when, for example, the charged lepton that is produced along with the subject neutrino for a particular experiment is only coupled to significantly by two mass eigenstates. In this case the mixing of the flavour eigenstates is given by:

$$\begin{pmatrix} \nu_\alpha \\ \nu_\beta \end{pmatrix} = \begin{pmatrix} cos\theta & sin\theta \\ -sin\theta & cos\theta \end{pmatrix} \begin{pmatrix} \nu_1 \\ \nu_2 \end{pmatrix} \tag{13}$$

where θ is known as the mixing angle and using the relation:

$$4\left|\sum_{i\pm} V^{*}_{\alpha i} V_{\beta i}\right|^{2} = sin^{2}2\theta \quad (14)$$

the probability for a neutrino to oscillate from the initial state ν_α to the state ν_β after travelling a distance L is:

$$P(\nu_\alpha \rightarrow \nu_\beta) = sin^{2}2\theta sin^{2}[1.27\Delta m^{2}(L/E)] \quad (15)$$

Equation (15) shows that for experiments such as MINOS that have a fixed[2]ratio L/E the amount of oscillation is dependant on just two parameters, the mising angle θ and the mass splitting Δm^2.

The above derivations considered neutrinos travelling through a vacuum. The implications of the passage of a neutrino through matter for its probabilities to oscillate to other flavours are known as the Mikheyev-Smirnov-Wolfenstein (MSW) effect [5][6]. The MSW effect considers the coherent forward scattering of neutrinos from particles they encounter as they traverse a medium. This can have observable effects for electron neutrinos (and anti-neutrinos) that, in addition to the neutral current interaction open to all neutrino flavours with quarks and electrons, have an additional charged current interaction $\nu_e + e^- \rightarrow (W^+ \rightarrow) e^- + \nu_e$. As such the MSW effect is of great importance for the study of *solar* neutrinos due to the high electron density of the sun but has no effect on the MINOS experiment which uses a beam almost entirely comprised of muon neutrinos.

Using equation (15) with the MINOS baseline of 735km, $sin^2 2\theta = 1$ (maximal mixing) and $\Delta m^2 = 2.5 \times 10^{-3}$ the survival probability of a ν_μ as a function of energy is shown in figure [4] at the end of this report.

3 The MINOS Experiment

The MINOS experiment utilises a beam of muon neutrinos produced at Fermilab in Chicago that are fired 735km through the Earth's crust towards the Soudan Mine in Minnesota. The beam is sampled first using the Near Detector situated on-site at Fermilab and then once again using the Far Detector at Soudan. A comparison of the neutrino event rates and spectra for charged current (CC) and neutral current (NC) interactions at these two detectors will be used in the MINOS physics analysis. This section will briefly describe the beam, detectors, the main physics objectives of the MINOS experiment and the need for a precise measurement of the neutrino flux.

[2]The neutrinos are not mono-energetic but they are peaked at a central value that depends upon the running conditions of the experiment.

3.1 The NuMI (Neutrinos at the Main Injector) Beam

The NuMI beamline takes 120GeV protons from the Main Injector at Fermilab and brings them to focus on a graphite target. Some of the produced charged hadrons (π^+s and K^+s) are then focussed by magnetic horns such that when they subsequently decay the resultant muon neutrinos are travelling along a path that passes through the Near and Far Detectors. A section of absorber and rock removes the μ^+s produced along with the neutrinos and the beam intercepts the Near Detector about 1km downstream from the target. The distance between the target and magnetic horns can be changed so as to modify the neutrino energy spectrum incident on the detectors and alter the oscillation parameter space to which MINOS is sensitive. A more detailed description of the NuMI beam can be found in [7].

3.2 The Detectors

The Near and Far Detectors are both fine grained tracking calorimeters that use a series of planes of steel and plastic scintillator sandwiched together and are magnetized with a $\sim$1.5T magnetic field. The detectors are designed to be as similar as possible so as to reduce systematic errors but with electronics that can account for the vast difference in event rates (the MINOS Near Detector features a 'deadtimeless' readout). Calibration of the detectors is achieved using a light injection system and a third Calibration Detector that stood in a test beam from the CERN Proton Synchrotron (PS) and the results of which characterise the individual detector responses to the passage of a variety of particles. A more detailed description of the MINOS detectors can be found in [8].

3.3 Physics Goals

The primary physics goal of the MINOS experiment is to confirm neutrino oscillations as the mechanism responsible for the apparent loss of atmospheric ν_μ and to precisely measure the parameters governing these oscillations. There are several independant and parallel measurements that MINOS can make to achieve these aims; statistical tests, spectral comparisons and appearance searches.

In the *T-Test* neutrino events are first classified as long or short where long events could be defined as those that contain a muon in the final state (ν_μ CC). The following ratio can then be constructed as a function of energy:

$$T = \frac{\left(\frac{N_L}{N_L+N_S}\right)_{\text{far}}}{\left(\frac{N_L}{N_L+N_S}\right)_{\text{near}}} \tag{16}$$

where $N_{L/S}$ denotes the number of long or short events measured. Any statistically significant deviation of T from unity would be a sign for oscillations. T is also a useful quantity as it removes the problem of differing event rates at the two detectors and is doubly sensitive to oscillations via both the disappearance of ν_μ (long events) and the appearance of ν_e or ν_τ (short events).

The most sensitive measurement available to MINOS for the determination of oscillation parameters is the comparison of ν_μ CC energy spectra at the near and far detectors. The spectrum from the Near Detector can be measured and using Monte Carlo a predicted spectrum for the Far Detector assuming no oscillations can be derived. If the ratio of this predicted spectrum with the measured Far Detector spectrum is taken and results in a deviation from unity with a 'dip' around some energy then the value of the mixing angle θ_{23} is related to the size of this depletion and the value of the mass splitting Δm^2_{23} is related to the mean energy of the missing ν_μ. Figure [5] shows Monte Carlo reconstructed energy distributions with and without oscillations for the MINOS low energy beam configuration (peak $\sim$ 3GeV) and the ratios of these distributions.

It was originally thought that MINOS could search for the appearance of both ν_e and ν_τ but the values of the oscillation parameters suggested by the likes of Super-Kamiokande have become low enough such that the peak in the MINOS energy spectrum will need to be lower ($\sim$ 1.5GeV) than the threshold for τ production ($\sim$ 4.0GeV). MINOS does have some sensitivity to differentiate between hadronic and electromagnetic showers and should be able to detect ν_e appearance and improve the current CHOOZ limit [9] on another of the mixing angles, θ_{13}. Measurements of θ_{13} are becoming increasingly important as its value will determine the possibility of observing CP violation in the leptonic sector.

3.4 The Neutrino Flux

The most powerful measure of the oscillation parameters that MINOS can offer is dependant upon taking the unoscillated neutrino energy spectrum from the Near Detector and translating this to an unoscillated spectrum at the Far Detector. A large error is introduced into the spectral comparison if the error on the Near Detector spectrum is large. The main source of error for the Near Detector neutrino energy spectrum is the size of the incident neutrino flux (as a function of energy) and it is crucial for the MINOS measurement of the oscillation parameters that the error on this neutrino flux is as small as possible.

4 Quasi-Elastic Neutrino Events and Estimating the Neutrino Flux

4.1 Neutrino-Nucleon Cross Sections

The MINOS L/E ratio is such that to search for oscillation parameters in the region of parameter space suggested by experiments such as Super-Kamiokande the neutrino energy spectrum will need to be peaked at $\sim$ 2GeV. In this region of energies the cross sections for quasi-elastic scattering (QE), resonance production (RES) and deep-inelastic scattering (DIS) neutrino-nucleon interations will all make a significant contribution to the observed events as shown in figure[6]. The following Feynman cartoons illustrate the main QE, RES and DIS interactions that will occur in MINOS:

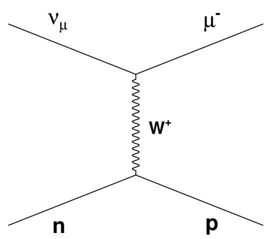

Figure 1: $\nu_\mu n \to \mu^- p$ *In a QE event the neutrino is considered to scatter off an entire nucleon rather than it's constituent partons and the target nucleus does not break up but is modified with a neutron turning into a proton. This proton is detectable as it will travel a short distance in the MINOS detectors.*

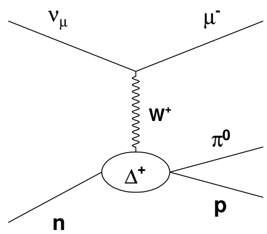

Figure 2: $\nu_\mu n \to \Delta^+ \to \mu^- p\pi^0$ *In a RES event the target nucleus does not break up but a resonance is formed which subsequently decays leaving a proton and a pion. Again the proton and pion are both observable in the detectors. MINOS will mostly see the Δ(1232) resonance.*

In the current formalism the QE cross section is calculable and a more detailed description of the phenomenology and modelling of QE events can be found in [10] and [11]. For a QE event with the following 4-momenta:

$$\nu_\mu(k_1) + N(p_1) \to \mu^-(k_2) + N(p_2) \tag{17}$$

the matrix element can be written:

$$\mathcal{M} = \frac{ig^2 cos\theta_c}{4}\frac{g_{\mu\nu}}{q^2 - M_W^2}\overline{u}(k_2)\gamma^\mu(1-\gamma_5)u(k_1)\overline{u}(p_2)\Gamma^\nu u(p_1) \tag{18}$$

and Γ^ν can be written:

$$\begin{aligned}\Gamma^\nu &= \gamma^\nu F_1^V(q^2) + i\sigma^{\nu\alpha}q_\alpha\frac{\xi F_2^V(q^2)}{2M} + q^\nu\frac{F_3^V(q^2)}{M} \\ &+ \gamma^\nu\gamma_5 F_A(q^2) + q^\nu\gamma_5\frac{F_P(q^2)}{M} + \gamma_5(p_1+p_2)^\nu\frac{F_3^A(q^2)}{M}\end{aligned} \tag{19}$$

where F_i^V ($i \in$(1,2,3)) are the weak vector form factors of the nucleon, F_A,F_3^A are the weak axial-vector form factors of the nucleon, F_P is the pseudoscalar form factor of the nucleon, $\xi = k_p - k_n + 1$ where $k_{p/n}$ is the anomalous magentic moment of the proton or neutron and M is the mass of the struck nucleon.

The form factors are in general complex, however, they must all be real to preserve time reversal invariance and in addition F_3^A and F_3^V must be imaginary because of charge symmetry and so $F_3^A = F_3^V = 0$ (no second class currents and hence G-parity is conserved). According to the conserved vector current hypothesis (CVC) the vector current belongs to a triplet of conserved currents associated with the conservation of

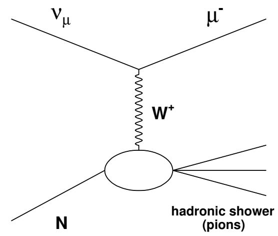

Figure 3: $\nu_\mu N \rightarrow$ *pions* *In a DIS event the momentum transfers involved are large and the target nucleus breaks up and forms a hadronic shower of pions.*

isospin in hadronic processes [12] and F_1^V and F_2^V can be related to the electromagnetic form factors which are much better measured using electron scattering experiments. These weak vector currents can be written in terms of the Sachs form factors:

$$F_1^V(q^2) = \frac{G_E^V(q^2) - \frac{q^2}{4M^2} G_M^V(q^2)}{1 - \frac{q^2}{4M^2}} \tag{20}$$

$$\xi F_2^V(q^2) = \frac{G_M^V(q^2) - G_E^V(q^2)}{1 - \frac{q^2}{4M^2}} \tag{21}$$

where using dipole forms:

$$G_E^V(q^2) = \frac{1}{(1 - \frac{q^2}{M_V^2})^2} \qquad G_M^V(q^2) = \frac{1+\xi}{(1 - \frac{q^2}{M_V^2})^2} \tag{22}$$

where M_V is the vector mass. By analogy with this vector case the axial-vector current can be written using a dipole form as follows:

$$F_A(q^2) = \frac{F_A(0)}{(1 - \frac{q^2}{M_A^2})^2} \tag{23}$$

where M_A is the axial vector mass. Using the partially conserved axial current hypothesis (PCAC) [13] a reasonable form for F_P at all q^2 is:

$$F_P(q^2) = 2M^2 \frac{F_A(q^2)}{M_\pi^2 - q^2} \tag{24}$$

where M_π is the charged pion mass. The QE differential cross section with respect to q^2 can then be derived and looks as follows[3]:

[3] This is the equation for neutrinos. For anti-neutrinos the term $F_A(F_1^V + \xi F_2^V)$ must be replaced with $-F_A(F_1^V + \xi F_2^V)$.

$$
\begin{aligned}
\frac{d\sigma}{d|q^2|} &= \frac{G_F^2 cos^2\theta_c}{8\pi E_\nu^2} \qquad [(F_1^V)^2 \frac{q^4 - 4M^2(m_l^2 - q^2) - m_l^4}{4M^2} \\
&+ (\xi F_2^V)^2 \frac{4M^2(q^4 - m_l^4) - q^4(m_l^2 - q^2)}{16M^4} + (F_A)^2 \frac{q^4 + 4M^2(m_l^2 - q^2) - m_l^4}{4M^2} \\
&- (F_P^2) \frac{m_l^2 q^2(-q^2 + m_l^2)}{4M^2} + F_1^V \xi F_2^V \frac{2q^4 + q^2 m_l^2 + m_l^4}{2M^2} - F_A F_P \frac{m_l^2(-q^2 + m_l^2)}{2M^2} \\
&+ F_A(F_1^V + \xi F_2^V) q^2 \frac{s-u}{M^2} + \left((F_1^V)^2 - \frac{(\xi F_2^V)^2 q^2}{4M^2} + (F_A)^2 \right) \frac{(s-u)^2}{4M^2}] \qquad (25)
\end{aligned}
$$

where G_F is the Fermi coupling, m_l is the mass of the produced charged lepton and $s - u = 4E_\nu M + q^2 - m_l^2$ using the usual Mendelstam variables. A toy model was constructed according to the above formula so as to read in energies and momentum transfers and give out the differential cross section. Using numerical integration methods over an appropriate range in q^2 (determined from the kinematics of the QE process) the total QE cross section was then evaluated over a range in initial neutrino energies. This toy model does not include effects such as Pauli blocking of nucleons in the nucleus or the intranuclear rescattering of protons and pions. This model is not quite performing as expected but should show that the QE cross section is almost flat with energy down to about 1GeV. Figure [6] shows this shape along with a variety of data points from many different experiments.

4.2 Using QE Events for a Flux Estimate

The cross section for QE neutrino-nucleon interactions has a well known shape and is flat with energy down to about ∼1GeV whereas the overall normalisation of this cross section is relatively uncertain (as suggested by the data points on figure [6]). However, the cross section for DIS neutrino-nucleon interactions is fairly well known at energies of ∼10-20GeV and as such the neutrino flux incident on the NuMI target at these energies can be evaluated by 'dividing out' the cross section from an estimator of the numbers of DIS events at these energies. The flux measured using DIS events can then be used to 'pin' the normalization of the QE cross section at these energies and using the flat shape of this cross section the flux can then be evaluated as a function of neutrino energies (∼1-20GeV) using estimators for the numbers of QE events measured in a set of bins of reconstructed neutrino energy. This method relies on attaining relatively pure samples of QE events over a range of energies with backgrounds that can be understood and accounted for.

4.3 QE Sample Selection

4.3.1 Discriminating Variables

The first step in selecting QE events is to discern a number of variables that can distinguish in some way between these events and the backgrounds of RES,DIS and NC events. In the following a high statistics Monte Carlo (MC) sample of neutrino events was generated with a flat energy spectrum (1/E flux) between 0-20GeV. Figure [8] shows the decomposition of the reconstructed energy spectrum of these events into the various processes.

The first variables considered were high level reconstructed quantities. The numbers of reconstructed showers and tracks per event are useful for background rejection. An event with no showers is most likely QE where the proton has been re-absorbed in the nucleus or is not seen in the detector whereas RES,DIS and NC events are more likely to have hadronic showers. In contrast an event with no track is likely not to be QE but a RES,DIS or NC event where the track has been combined with a large shower by the reconstruction software (or an NC event where there was no muon produced). Distributions of these variables for the various event types and for various ranges of reconstructed neutrino energy can be found in figures [9] and [10].

A more powerful high level quantity that is useful for process discrimination is the reconstucted invariant mass squared. For QE events this is approximately the square of the proton mass and the MINOS detectors can provide a relatively good resolution of this peak. For RES events there is a less well defined peak corresponding to the squared mass of the $\Delta(1232)$ and for DIS events the invariant mass squared is on average higher still. Figure [11] shows invariant mass squared distributions for CC event processes for 4 bins of reconstructed neutrino energy.

The above variables can be useful but a good discrimination can also be achieved by considering the topology and charge distribution of hits near to the event vertex. A set of variables were developed that rely on the removal of the main muon track from an event. For each event if a track is found by the MINOS standard reconstruction software (SR) then the hits corresponding to this track are removed from further consideration. For hits that are flagged as being shared between a track and a shower by the SR the hit is kept but has the equivalent of one minimum ionizing particle (MIP) subtracted from its pulse height (PH). Protons and pions will not travel more than a couple of metres in the MINOS detectors and so in addition to this procedure if a hit is more than 2m from the event vertex (from SR) it is removed. Finally, in an effort to remove cross-talk between PMT pixels in the detector, hits were also required to have at least a certain minimum PH to be considered in the following variables.

Figure [12] shows the total PH remaining in the event after the above hit removal steps. The QE events have little remaining PH, as the proton does not produce much hadronic showering, with higher PH for RES and then DIS events corresponding to a single π_0 and multiple pions respectively.

NC events do not tend to have a track reconstructed and this would mean that they should occur away from the QE events in the above variable. However, for NC events only a small fraction of the initial neutrino energy is seen and so they tend to appear lower in this remaining PH variable. One way to remove them from a QE-like sample is to then take this remaining PH as a fraction of the total event PH before any hit removal steps. In this variable NC events will have values close to unity. QE events will have low values with RES and DIS higher respectively as shown in figure [13].

Another useful variable is the number of high PH hits that remain after the removal steps. Protons from QE and RES events will only leave a few large hits in the detector whereas pions from RES and DIS events will range out further in the detector and leave a larger number of high PH hits as shown in figure [14].

The final variable to be described here is obtained by perfoming a Hough transform over the remaining hits in an event. It is hard to actually see short tracks from the event vertex corresponding to the protons and pions with the Hough method but the height of the peak in Hough space is useful for process separation and can be thought of as characterising the spatial maximum of the hadronic system at the event vertex. This variable is lower for QE events than for RES and DIS as would be expected from the relative amounts of hadronic showering for these processes and as shown in figure [15].

4.3.2 A Maximum Likelihood Based Sample Selection

All of the variables presented above scale with energy and so it was decided to perform a separate maximum likelihood analysis (based upon the above variables) in a series of bins of reconstructed neutrino energy. In addition it was decided to bin the [0,20]GeV range in asymmetric bins so as to account for the MINOS Near Detector's energy resolution.

The variables were checked for correlations and it was decided to combine the PH remaining after the hit removal steps and the number of high PH hits into a single variable using a simple principal components analysis. As such there are five one-dimensional distributions created for each type of event process in each reconstructed neutrino energy bin and these are normalised and used as probability distributions functions (PDFs) in the likelihood analysis. The resulting probabilities for an event are used to construct a particle identification (PID) parameter according to:

$$P_{PID} = -\sqrt{-log(P_{QE})} + \sqrt{-log(P_{bg})} \tag{26}$$

where P_{PID} is the PID parameter for a particular event and $P_{QE/bg}$ are the compound probabilities for the event to be QE or RES/DIS/NC defined by:

$$\begin{aligned} P_{QE} &= \sum_{i=1}^{5} P_{i,QE} \\ P_{bg} &= \sum_{i=1}^{5} P_{i,RES} + \sum_{i=1}^{5} P_{i,DIS} + \sum_{i=1}^{5} P_{i,NC} \end{aligned}$$

where $P_{i,X}$ is the probability from the i^{th} PDF for event process X. The method has been tested using the MC sample illustrated in figure [8]. Figure [8] also demonstrates the asymmetric bin structure of the likelihood analysis with bin ranges ranging from 0.5GeV to 3GeV. The first half of the events were used to create the PDFs and the second half of the events were analysed and their corresponding PID parameter values evaluated. All events were subject to the same series of cuts before being used:

- Event vertex must be contained in the fiducial volume.
- There must be only one track present in the event.
- This track must pass a track quality cut.
- The reconstructed neutrino energy must be greater than zero.

Figure [16] shows the distributions of this PID parameter for a selection of reconstructed neutrino energy bins and for QE events and non-QE events. The QE-like sample was then extracted by defining an independent cut on the PID parameter in each bin above which events are classified QE-like. The cut values were tuned to give a flat efficiency and as such the distribution of QE-like events should reflect the shape of the input neutrino flux (which was 1/E) given the flat shape of the QE cross section. Figures [17] and [18] show the QE efficiencies and purities of this sample as well as the distributions of numbers of events with energy for the various processes before and after the QE-like sample selection.

The method produces a sample of good purity even at higher energies where the QE cross section only accounts for a very small number of events. The QE efficiency can be flattened and figure [18] shows that the shape of the selected events follows the expected 1/E distribution. The largest contamination in the sample comes from RES events at low energies but this could be further reduced with tighter PID cuts. The MINOS near detector will have a very large data set and so further reductions in efficiency can be tolerated to achieve high purity samples. The following section will detail one possible unfolding method to extract the neutrino flux as a function of energy and take into account the possible differences between reconstructed and true neutrino emergies.

4.4 Flux Extraction

For each reconstructed energy bin i an estimator can be contsructed for the number of true QE events in that bin according to:

$$\hat{n}_i = C_i(m_i - b_i) \tag{27}$$

where m_i is the number of measured events in bin i (from data), b_i is the number of expected background events in bin i (from MC) and C_i is the correction factor (or generalised efficiency) and can be expressed as:

$$C_i = \left(\frac{n_i}{r_i}\right) \tag{28}$$

where n_i is the number of true QE events in the true energy bin i and r_i is the number of QE-like events in reconstructed energy bin i (both from MC). If the reconstruction were perfect this would reduce to ε^{-1} where ε is the QE efficiency. Then using an appropriate fiducial volume the neutrino flux for each bin can be evaluated by 'dividing out' the value of the cross section in that energy bin. This process has not been carried out yet but has high priority for the near future.

5 Preliminary Look at Near Detector Data

The last few months have proved to be a very exciting time for MINOS and a major focus for the experiment has been to see if Near Detector MC is accurately explaining Near Detector data. The QE-like sample selection analysis was applied to the data for the MINOS medium energy beam configuration (peak ~5GeV) and a corresponding MC data set. The data and MC now have far less events in the very low energy region and high energy regions compared to the MC that was used to evaluate the sample selection and as such it was not possible to create PDFs for the whole 0-20GeV energy range. The QE-like sample has neutrinos with reconstructed energy between 2-10GeV but is still expected to have a QE purity of ~70%. In the data and MC comparisons that follow the samples have been normalised to the number of protons hitting the NuMI target (POTs).

Figure [19] shows the reconstructed muon energy of the QE-like events and seeing as there is very little hadronic showering for such events this can also be thought of as the reconstucted neutrino energy itself. This figure shows that in data the reconstructed muon energy is ~0.5GeV lower than in the MC. This effect looks consistent over the energy range of the plot but is still relatively small.

Figures [20] and [21] show the reconstructed Q^2 for the samples. They reveal that there seems to be a suppresion in the numbers of events in the data at low Q^2. This is only a preliminary result and the MC does not accurately explain the data yet but a simliar suppression at low Q^2 has been seen by both MiniBooNE and K2K. These experiments note that the suppression is greater than what is expected from Pauli blocking in the nucleus and ask the question 'is there some interseting physics at work here'.

6 Conclusions and Further Work

There is great need for an accurate measurement of the neutrino flux for MINOS and a method for determining this flux as a function of neutrino energy using QE events has been described. A maximum likelihood analysis using PDFs from a set of 5 variables in a series of reconstucted neutrino energy bins has been developed to select the QE-like sample and has been shown to work well. The methodolgy for unfolding the neutrino flux from this sample has been suggested but not tested. The next steps are to produce flux results for Near Detector MC and then to begin to work with the data itself. In addition some preliminary data and MC comparisons have been made and these will now be repeated with higher statistics and any discrepancies investigated.

References

[1] K. S. Hirata *et al.* [Kamiokande II Collaboration], Phys. Lett. B **280** (1992) 146

[2] W. W. Allison *et al.* [Soudan-2 Collaboration], Phys. Lett. B **449** (1999) 137

[3] B. Pontecorvo, Sov. Phys. JETP **26** (1968) 984 [Zh. Eksp. Teor. Fiz **53** (1967) 1717]

[4] G. Fogli, E. Lisi and G. Scioscia, Phys. Rev. D **52** (1995) 5334

[5] L. Wolfenstein, Phys. Rev. D **17** (1978) 2369

[6] S. Mikheyev and A. Smirnov, Sov. J. Nucl. Phys **42** (1986) 913 [Yad. Fiz. **42** (1985) 1441]; Sov. Phys. JETP **64** (1986) 4 [Zh. Eksp. Teor. Fiz **91** (1986) 7]

[7] The MINOS Collaboration, *The NuMI Beam Technical Design Report*, Technical report, Fermilab 1999

[8] The MINOS Collaboration, *The MINOS Technical Design Report*, Technical report, Fermilab 1999

[9] M. Apollonio *et al.* [CHOOZ Collaboration], Phys. Lett. B **466** (1999) 415

[10] C. H. Llewellyn Smith, Phys. Rep. **3** (1972) 261

[11] E. A. Paschos and J. Y. Yu, Phys. Rev. D **65** (2002) 033002

[12] R. P. Feynman and M. Gell-Mann, Phys. Rev. **109** (1958) 193

[13] M. Gell-Mann and M. Levy, Nuovo Cimento **16** (1960) 705

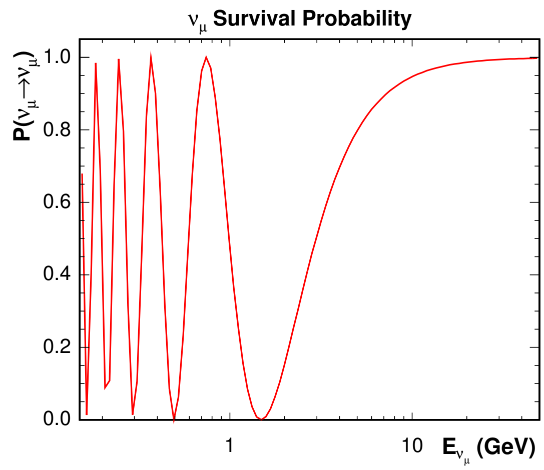

Figure 4: *The survival probability of ν_μ as a function of neutrino energy. The first dip occurs at ~1.5 GeV and it is the effects of this first dip to which the MINOS experiment will be sensitive. The depth and width of the dip are related to the oscillation parameters θ and Δm^2.*

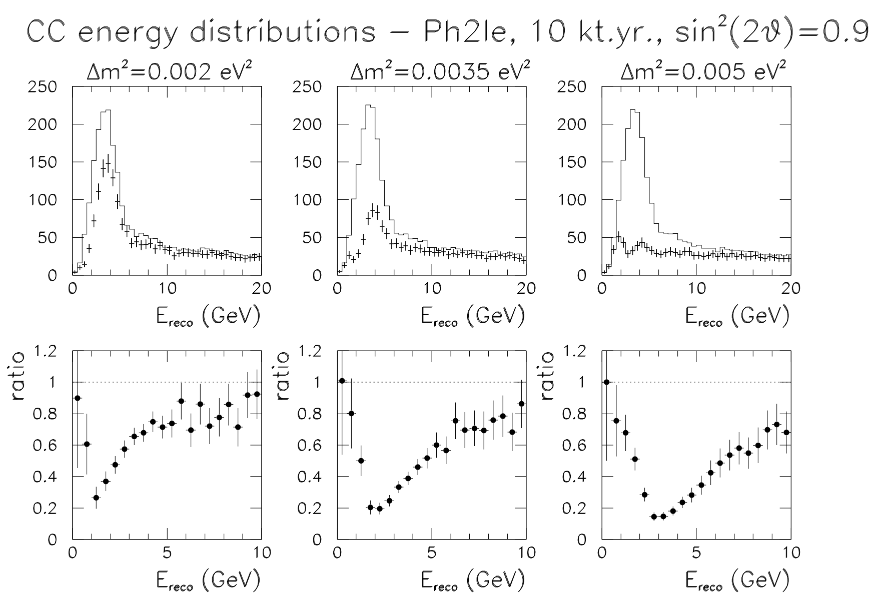

Figure 5: *The top row solid line histograms show unoscillated ν_μ CC energy spectra whilst the top row MC data point histograms show the oscillated spectra with a mixing angle of $\sin^2 2\theta = 0.9$ and three different Δm^2 values. The bottom row of plots show the ratio of these spectra. All the plots assume a 10 kiloton year exposure and include the effects of mis-identified NC events and a smearing of the true neutrino energies with a realistic resolution function.*

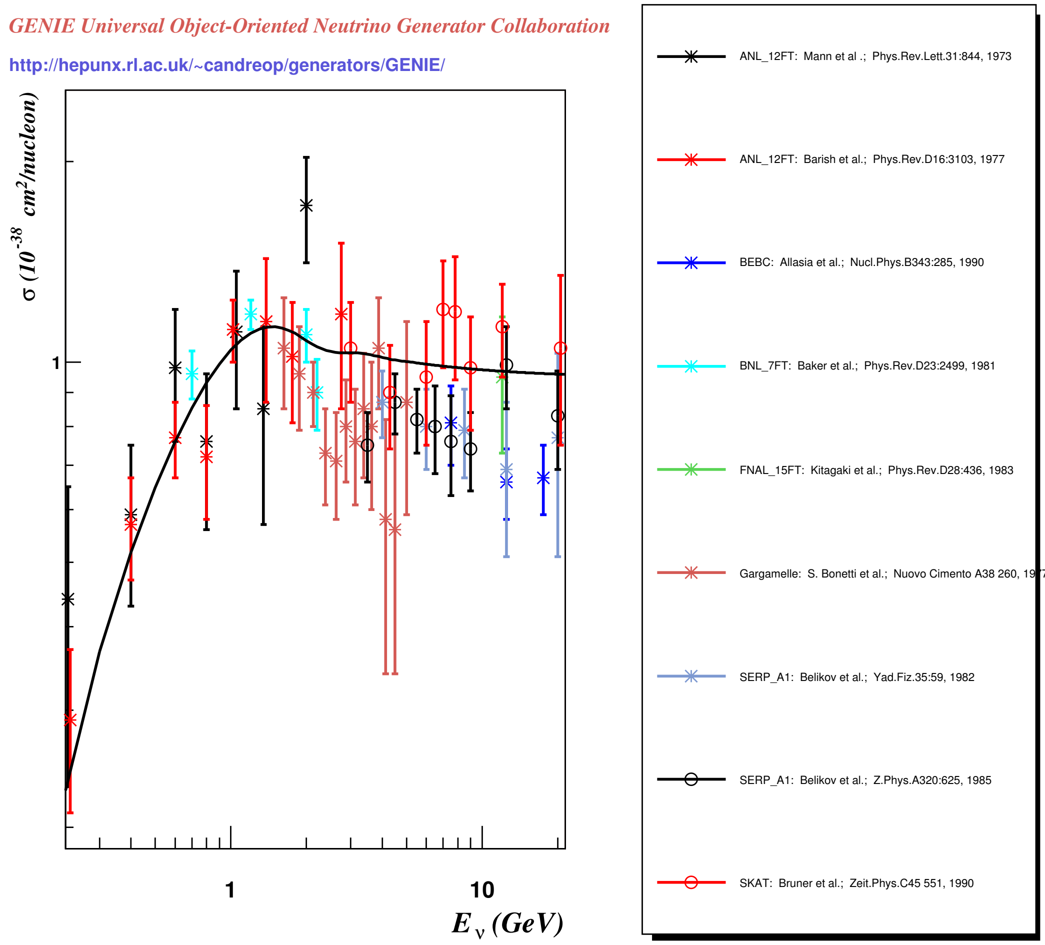

Figure 6: *QE cross section for muon neutrinos as a function of energy (from the GENIE collaboration).*

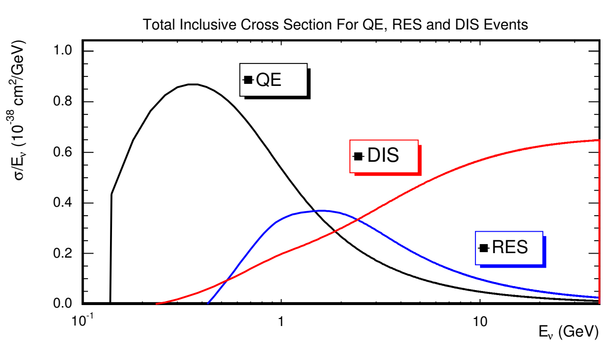

Figure 7: *Total inclusive cross section for different event types as a function of energy.*

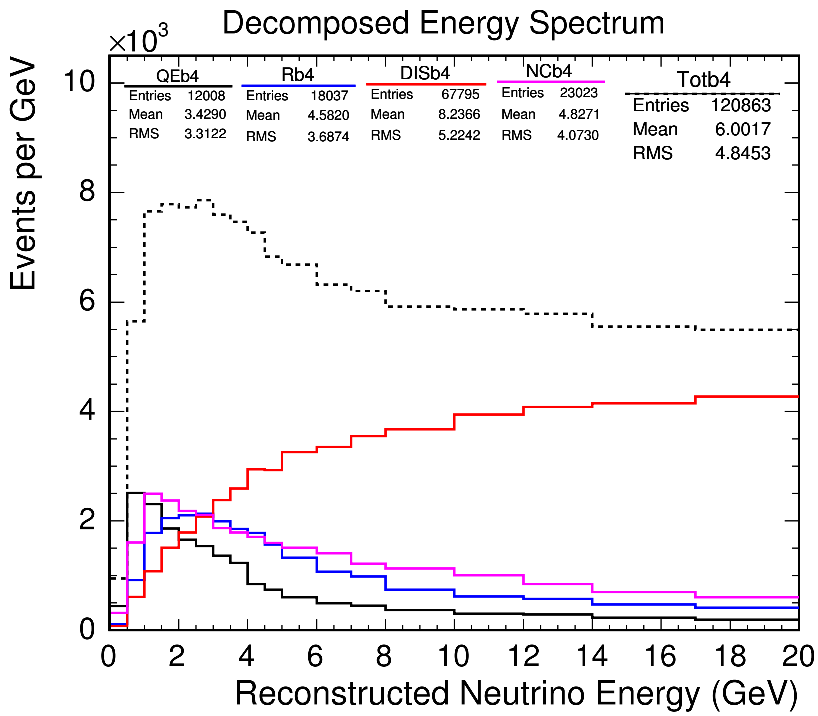

Figure 8: *Decomposed reconstructed neutrino energy spectrum. The spectrum is peaked reflecting the shape of the total cross section.*

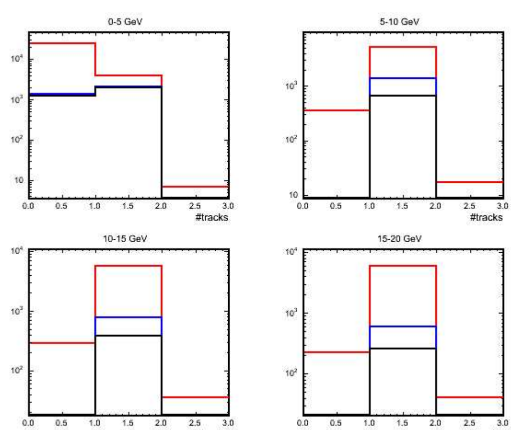

Figure 9: *Numbers of tracks for different event processes in 4 bins of reconstructed neutrino energy (Black=QE, Blue=RES, Red=DIS).*

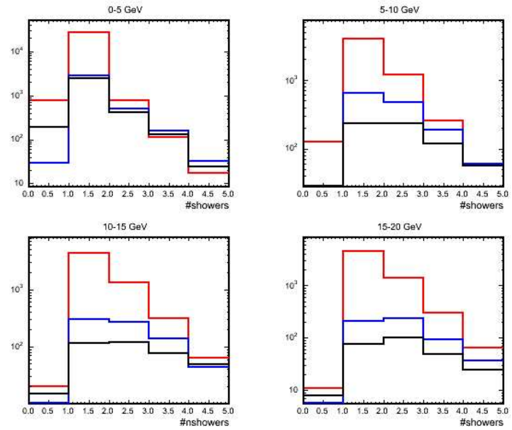

Figure 10: *Numbers of showers for different event processes in 4 bins of reconstructed neutrino energy (Black=QE, Blue=RES, Red=DIS).*

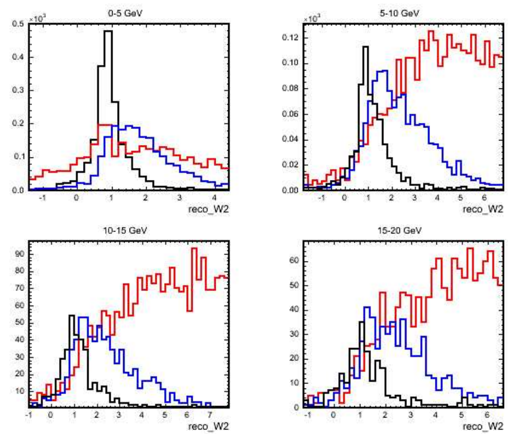

Figure 11: *Reconstructed invariant mass in (GeV)^2 for different event processes in 4 bins of reconstructed neutrino energy (Black=QE, Blue=RES, Red=DIS).*

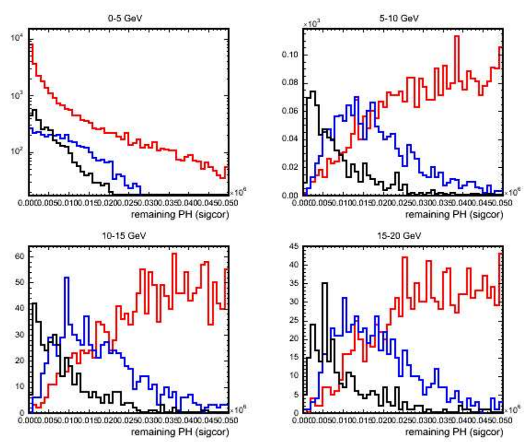

Figure 12: *Total remaining PH for different event processes in 4 bins of reconstructed neutrino energy (Black=QE, Blue=RES, Red=DIS).*

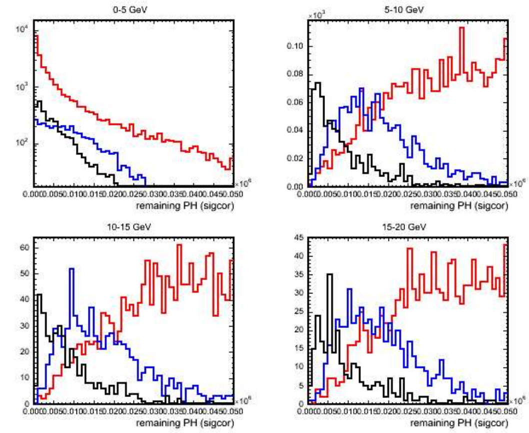

Figure 13: *Fractional remaining PH for different event processes in 4 bins of reconstructed neutrino energy (Black=QE, Blue=RES, Red=DIS).*

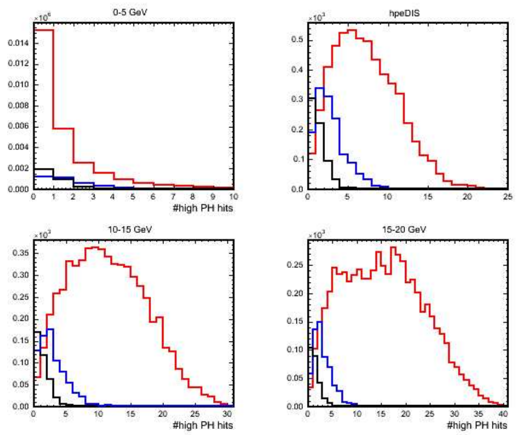

Figure 14: *High PH hits remaining for different event processes in 4 bins of reconstructed neutrino energy (Black=QE, Blue=RES, Red=DIS).*

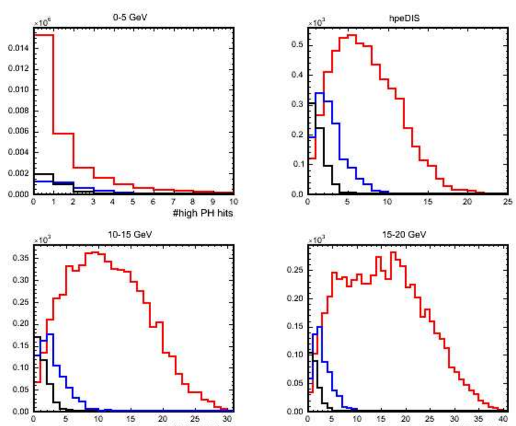

Figure 15: *Hough peak height for different event processes in 4 bins of reconstructed neutrino energy (Black=QE, Blue=RES, Red=DIS).*

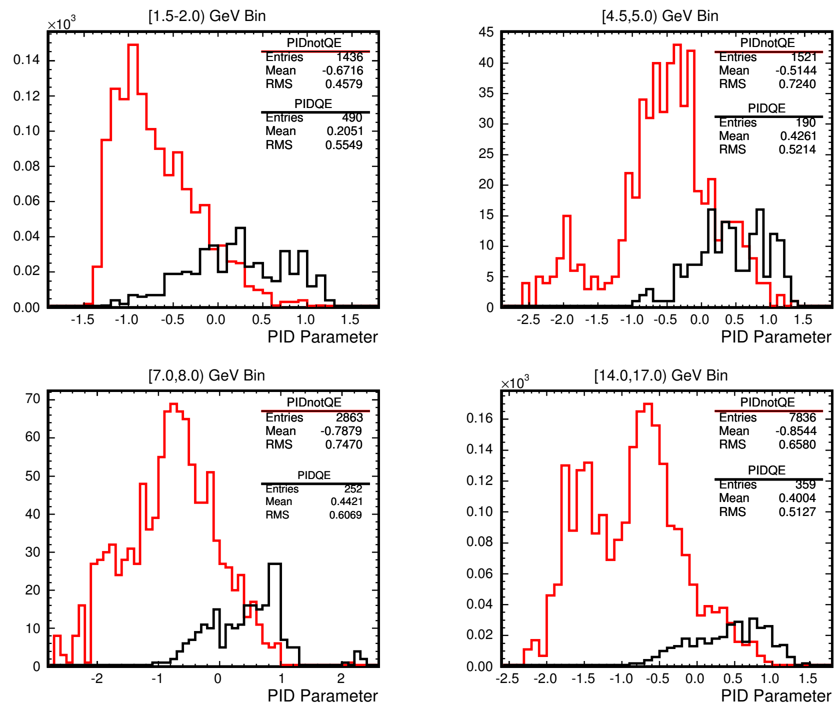

Figure 16: *PID parameter distributions for QE and non-QE events in a sampling of reconstructed neutrino energy bins (Black=QE, Red=non-QE).*

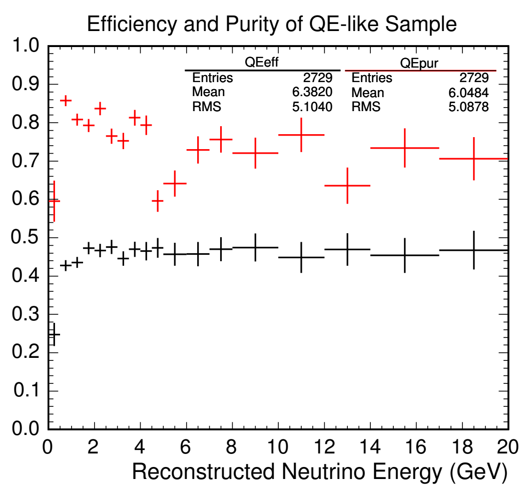

Figure 17: *QE efficiency (black) and purity (red). The purity starts off high where the QE cross section is peaked and then drops as the RES and DIS cross sections give a bigger fraction of the events and have energies at which it is harder to discriminate. The purity then rises again as the RES cross section dies off and the DIS events become easier to remove from the sample.*

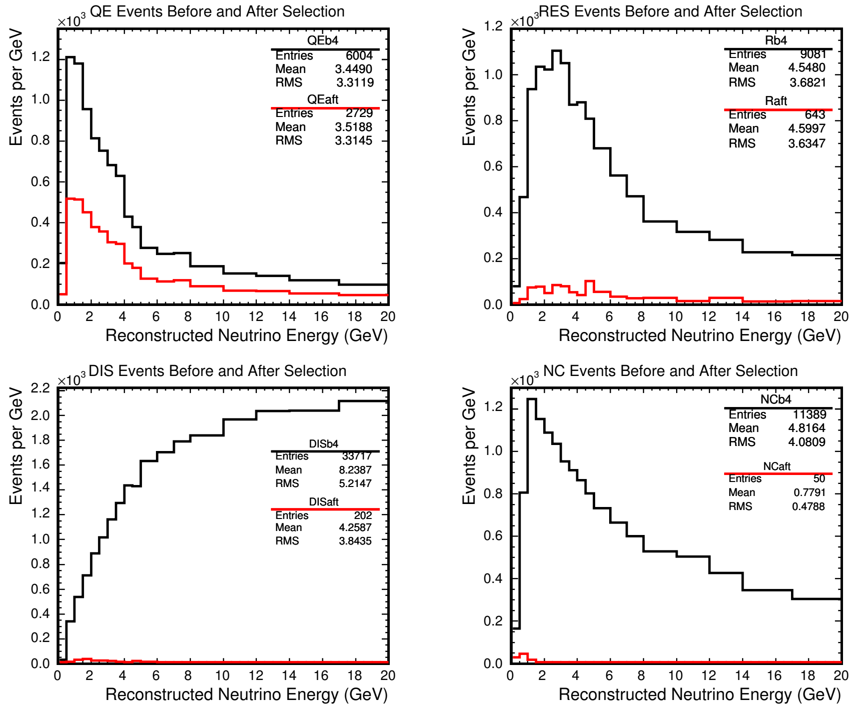

Figure 18: *Numbers of events before and after sample selection for QE, RES, DIS and NC. Only very small numbers of low energy DIS and NC events make it through to the QE-like sample. The majority of the impurity in the sample is from the lower energy RES events.*

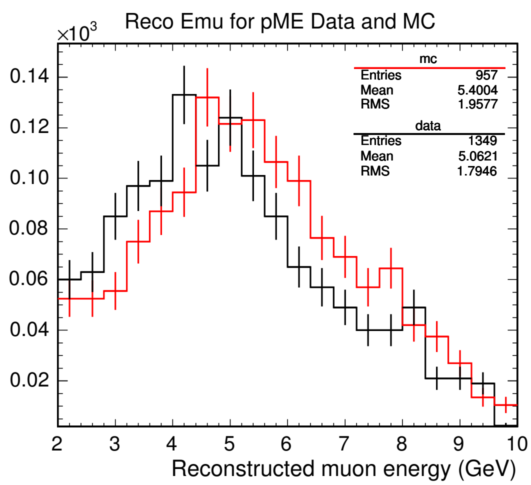

Figure 19: *A comparison of the reconstructed muon energy for Near detector data (black) and MC (red).*

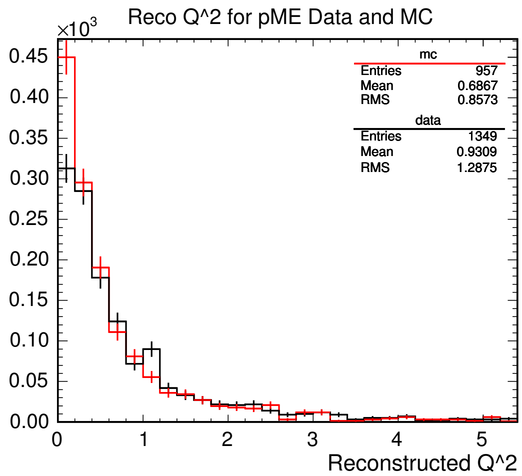

Figure 20: *A comparison of the reconstructed Q^2 for Near detector data (black) and MC (red).*

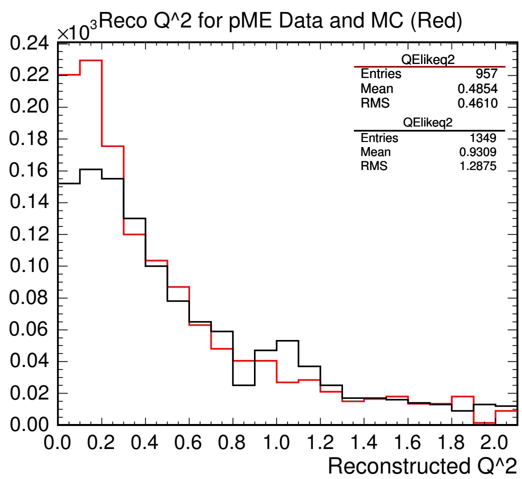

Figure 21: *A blow-up of the low Q^2 region.*